If $\omega\tau \gg 1$, ϵ can be simplified to

$$\epsilon(\omega) \approx 1 - \frac{\omega_p^2}{\omega^2}, \tag{13.4}$$

while the imaginary part is negligible.

If this approximation is valid around ω_p, the material is transparent for $\omega > \omega_p$ ($\epsilon > 0$). For $\omega < \omega_p$, ϵ becomes negative, *i.e.* the refractive index is purely imaginary and the material therefore has a reflectivity of 1. In this case, the material changes dramatically from transparent to reflective, as ω_p is crossed.

If the approximation $\omega\tau \gg 1$ is not valid, $\Im\chi$ cannot be neglected. The imaginary part will increase with decreasing frequency, *i.e.* with increasing wavelengths the absorption increases. For wavelengths longer than the plasma wavelength the material becomes more reflective, what we also see in Fig. 13.2. For application in solar cells, the TCO should be highly transparent in the active region of the absorber. Therefore the plasma-wavelength should at least be longer than the bandgap wavelength of the absorber. On the other hand the plasma frequency is proportional to the free carrier density N_f. A longer plasma wavelength therefore corresponds to a lower N_f. Finding an optimum between high transparency and high carrier densities is an important issue in designing TCOs for solar cell applications.

Even though the Drude model gives a good approximation of the free carrier related phenomena in TCOs, this model often is too simple. Therefore several authors used extended Drude models with more parameters [57–59].

Of all TCO materials currently available, the trade off between transparency and conductivity is best for indium tin oxide [60]. However, indium is a rare earth element with a very low abundance of 0.05 ppm in the Earth's crust, similar to the abundance of silver (0.07 ppm) and mercury (0.04 ppm) [61], which makes it less preferable for cheap large-scale PV applications. Therefore other TCO materials are thoroughly investigated and used in industry. Amongst them are aluminium doped zinc oxide, boron doped zinc oxide and fluorine doped tin oxide. The abundances of the used elements are: aluminium: 7.96%, zinc: 65 ppm, boron: 11 ppm, fluorine: 525 ppm, and tin: 2.3 ppm [61].

Often, TCOs in thin-film solar cells are nanotextured. These textures scatter the incident light and hence help to prolong the average path length of the photons. As a consequence, the absorption in the absorber layer can be increased leading to an increased photocurrent density and hence efficiency. Some examples for nanotextured TCO layers are discussed in Appendix D.

13.2 The III-V PV technology

Of all the thin-film technologies, the III-V (speak three-five) technology results in the highest conversion efficiencies under both AM1.5 standard test conditions and concentrated sun conditions. Hence, it is mainly used in space applications and concentrator photovoltaics (CPV), which we discuss in Section 15.8.

As some concepts use a crystalline germanium or an GaAs wafer as substrate, it might not be considered as a real thin film PV technology, in contrast to thin-film silicon, CdTe, CIGS or organic PV, which we will discuss later in this chapter. However, the III-V based

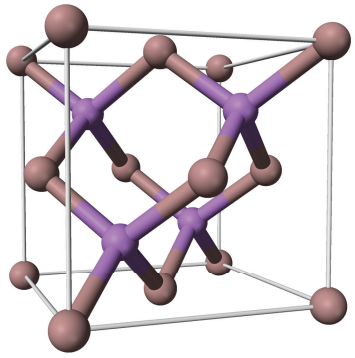

Figure 13.3: A unit cell of a gallium arsenide crystal in the zincblende structure [62].

absorber layers themselves can be considered as thin compared to the thickness of crystalline silicon wafers.

The III-V materials are based on the elements with *three valence electrons* like aluminium (Al), gallium (Ga) or indium (In) and elements with *five valence electrons* like phosphorus (P) or arsenic (As). Various different semiconductor materials such as *gallium arsenide* (GaAs), *gallium phosphide* (GaP), *indium phosphide* (InP), *indium arsenide* (InAs), and more complex alloys like GaInAs, GaInP, AlGaInAs and AlGaInP have been explored.

We now will take a closer look on GaAs, which is the most common III-V semiconductor for solar cells. GaAs has a *zincblende crystal structure*, illustrated in Fig. 13.3. It is very similar to the diamond cubic crystal structure with the difference that it has atoms of alternating elements at its lattice sites. In contrast to c-Si, where every Si atom has four neighbours of the same kind, in GaAs, every Ga has four As neighbours, while every As atom has four Ga neighbours. When compared to silicon, GaAs has a slightly larger lattice constant of 565.35 pm, and is significant denser than silicon with a density of 5.3176 g/cm^3 (Si: 543.07 pm, 2.3290 g/cm^3). Note that both Ga and As are are roughly twice as dense as silicon. In contrast to silicon, which is highly abundant, the abundance of gallium in the Earth's crust is only about 14 ppm [63]. GaAs therefore is a very expensive material. Arsenic is highly toxic; it is strongly suggested that GaAs is carcinogenic for humans [64].

Figure 13.4 shows the electronic band dispersion diagram of gallium arsenide. As mentioned before, GaAs is a *direct bandgap* material, *i.e.* , the highest energy level in the valence band is vertically aligned with the lowest energy level in the conduction band. Hence, only transfer of energy is required to excite an electron from the valence to the conduction band, but no transfer of momentum is required.

The bandgap of GaAs is 1.424 eV [24]. Here we look again at the absorption coefficient versus the wavelength. Consequently, as you can see in Fig. 12.4, the absorption coefficient of GaAs is significantly larger than that of silicon. The same is true for InP, another III-V material that also is shown in Fig. 12.4. Because of the high absorption coefficient, the same amount of light can be absorbed in a film more than one order of magnitude as thin when compared to silicon. Another advantage of the direct III-V semiconductor materials their sharp bandgap. Above E_g, the absorption coefficient increases quickly.

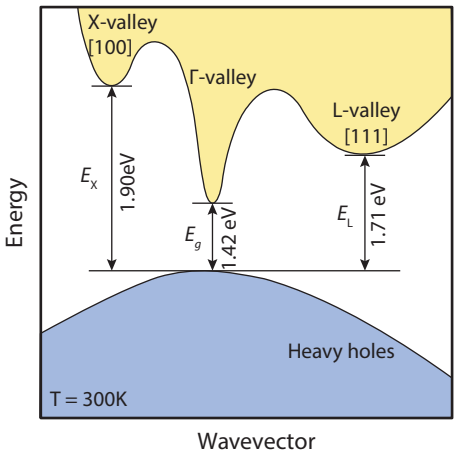

Figure 13.4: The electronic band dispersion diagram of gallium arsenide.

Let us now take a look at the utilisation of the bandgap energy. Since GaAs is a direct bandgap material, *radiative recombination processes* become important. On the other hand, Shockley-Read-Hall recombination can be kept at a low level because III-V films can be deposited by *epitaxy processes* that result in high purity films.

13.2.1 Multi-junction cells

III-V PV devices can reach very high efficiencies because they are often based on the multi-junction concept, which means that more than one bandgap is used. As discussed in Chapter 10, the maximum theoretical efficiency of single-junction cells is described by the Shockley-Queisser limit. A large fraction of the energy of the energetic photons are lost as heat, while photons with energies below the bandgap are lost as they are not absorbed.

For example, if we use a low bandgap material, a large fraction of the energy carried by the photons is not used. However, if we use more bandgaps, the same amount of photons can be used but less energy is wasted as heat. Thus, large parts of the solar spectrum and larges part of the energy in the solar spectrum can be utilised at the same time, if more than one *p-n* junctions are used.

In Fig. 13.5 a typical III-V triple junction cell is shown. As substrate, a germanium (Ge) wafer is used. From this wafer, the *bottom cell* is created. Germanium has a bandgap of 0.67 eV. The *middle cell* is based on GaAs with a gap of about 1.4 eV. The *top cell* is based on GaInP with a bandgap in the order of 1.86 eV.

Let now take a closer look on how a multi-junction solar cell works. Light will enter the device from the top. As the spectral part with the most energetic photons like blue light has the smallest penetration depth in materials, the junction with the highest bandgap always acts as the top cell. On the other hand, as the near infrared light outside the visible spectrum has the longest penetration depth, the bottom cell is the cell with the lowest bandgap.

Figure 13.6 shows the *J-V* curve of the three single *p-n* junctions. We observe *p-n* junc-

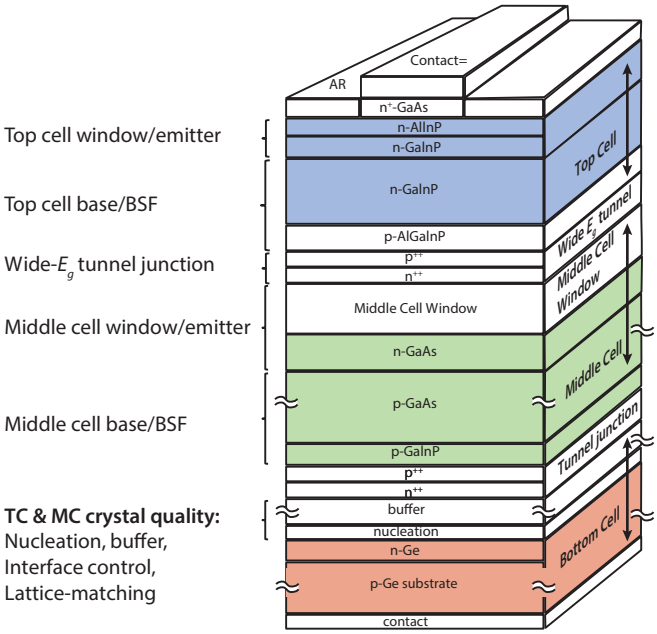

Figure 13.5: Illustrating a typical III-V triple junction solar cell.

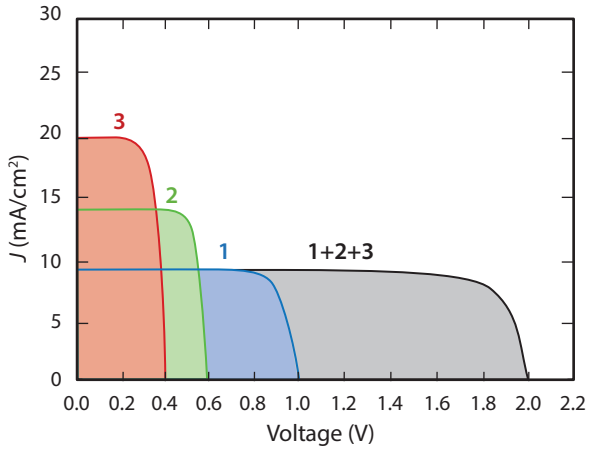

Figure 13.6: The *J-V* curves of the three junctions used in the III-V triple junction cell and *J-V* curves of the III-V triple junction cell (in black).

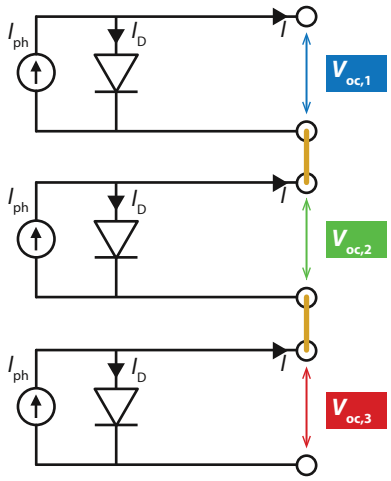

Figure 13.7: The equivalent circuit of the three junctions connected in series.

tion 1 has the highest open circuit voltage and the lowest short circuit current density, which means that this *p-n* junction has the highest bandgap. In contrast, *p-n* junction 3 has a low open circuit voltage and a high current density, consequently it has the lowest bandgap. *p-n* junction 2 has a bandgap in between. Hence, if we are designing a triple-junction cell out of these three junctions, junction 1 will act as the top cell, junction 2 will act as the middle cell and junction 3 will act as the bottom cell.

For understanding how the *J-V* curve of the triple junction looks like, we take a look at the equivalent circuit. Every *p-n* junction in the multi-junction cell can be represented by the circuit of a single-junction cell, as discussed in chapter 9. As the three junctions are stacked onto each other, they are connected to each other *in series*, as illustrated in Fig. 13.7. In a series connection, the voltages of the individual cell add up in the triple junction cell. Further, the current density in a series connection is equal over the entire solar cell, hence the current density is determined by the *p-n* junction generating the lowest current. The resulting *J-V* curve is also illustrated in Fig. 13.6. We see that the voltages add up and the current is determined by the cell delivering the lowest current.

Figure 13.8 (a) shows a typical band diagram of such triple junction. The top cell with high bandgap is shown at the left hand side and the bottom cell is at the right hand side. However, this band diagram does not represent reality. If we would place three *p-n* junctions in series, for example the *p*-layer of the top cell and the *n*-layer of the middle cell would form a *p-n* junction in the reverse direction than the *p-n* junctions of the three single junction solar cells. These reverse junctions would significantly lower the voltage of the total triple junction.

For preventing the creation of such reverse junctions, so-called *tunnel junctions* are included. These tunnel junctions align the valence band at one side with the conduction band at the other side of the tunnel junction, as illustrated in Fig. 13.8 (b). They have a high bandgap to prevent any parasitic absorption losses. Further, tunnel junctions are relatively thin and have an extremely narrow depletion zone. As a result, the slopes of the valence

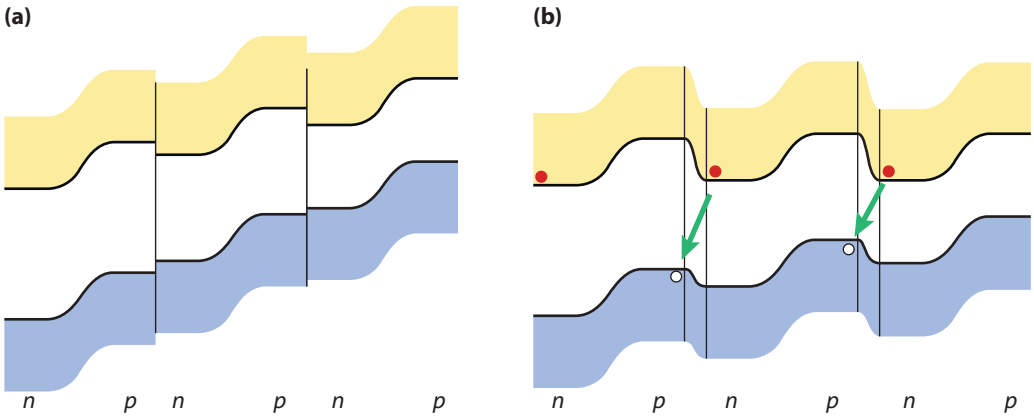

Figure 13.8: The band diagram of the III-V triple junction cell (a) without and (b) with tunnel junctions.

and conduction band are so steep that the electrons from n-layer can tunnel through the small barrier to the p-layer, where they recombine with the holes. It is important to have the tunnel junctions with a low resistance such that the voltage loss across them is low.

In the triple junction cell, two tunnel junctions are present. First, a tunnel junction via that the holes in the p-layer of the top cell have to recombine with the electrons of the n-layer of the middle cell. Secondly, a tunnel junction where the holes in the p-layer of the middle cell recombine with the electrons of the n-layer of the bottom cell. The electrons in the top cell n-layer are collected at the front contact and the hole in the p-layer of the bottom cell are collected at the back contact. It is important to realise that the recombination current at the tunnel junctions represents the current density of the complete triple junction.

Let us take a look at the external parameters of a typical lattice matched triple junction solar cell from SpectroLab, a subsidiary of The Boeing Company. Because this cell was developed for space applications, it is not tested under AM1.5 conditions, but under AM0 conditions with an irradiance of 135 mW/cm^2. The total open circuit voltage is 2.6 V. The short circuit current density is 17.8 mA/cm^2, which corresponds to a spectral utilisation up to the lowest bandgap (0.67 eV) of

$$J_{\text{tot}} = 3 \cdot 17.8 \text{ mA/cm}^2 = 53.4 \text{ mA/cm}^2. \tag{13.5}$$

The maximal theoretical current that could be generated when absorbing AM0 for all wavelength shorter than 1850 nm, which corresponds to 0.67 eV, is 62 mA/cm^2. The average EQE of the solar cell thus is 86%, which is an very impressive value. Further, this cell has a very high fill factor of 0.85, which means that it has a conversion efficiency of 29.5% under AM0 illumination.

Figure 13.9 shows the EQE of the subcells of a typical III-V triple junction cell. We note that the shape of the spectral utilisation of all the curves approaches the shape of block functions, which would be the most ideal shape. These block shapes are possible because the III-V materials have very sharp bandgap edges and high absorption coefficients. We see that the bottom cell generates much more current than the middle and top cells. Hence, a lot of current is lost in the bottom cell.

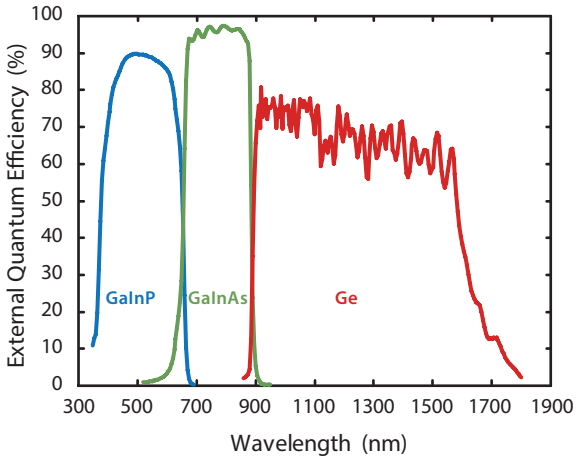

Figure 13.9: The external quantum efficiency of a three-junction III-V solar cell (Data from SPECTROLAB).

This ineffective use of the near infrared part can be reduced using quadruple junctions instead of triple junctions. In these cell, an additional cell is placed in-between the middle and bottom cells of the triple junction. The spectral utilisation can be even increased further by moving to multi-junction solar cells consisting of 5 or even 6 junctions. The major challenge for these cells is that lattice matching can not be guaranteed anymore. Lattice-mismatched multi-junctions are called *metamorphic multi-junctions*. They require buffer layers that have a profiling in the lattice constant, going from the lattice constant of one *p-n* junction to the lattice constant of the next *p-n* junction. Using this technology, Spectrolab could demonstrated 38.8% conversion efficiency of a 5-junction solar cell under 1-sun illumination [47].

The III-V PV technology is very expensive. Hence, such cells are mainly used for space-applications and in concentrator technology, where high performance is more important that the cost. Further, using concentrator photovoltaics (CPV), which is discussed in Section 15.8, allows to reduce the solar cell area drastically.

The current world record conversion efficiency for all solar cell technologies on lab scale is 46.0% for a four-junction III-V solar cell under 508-fold concentrated sun light conditions. This result was achieved by cooperation of Soitec and CEA-Leti, France, with the Fraunhofer Institute for Solar Energy Systems ISE [65].

13.2.2 Processing of III-V semiconductor materials

As already mentioned above, high quality III-V semiconductor materials can be deposited using *epitaxy* deposition methods. In this method, crystalline *o*verlayers are deposited on a crystalline substrate, such that they adopt the crystal lattice structure of the substrate. The *precursor* atoms from that the layers are grown are provided by various elemental sources. For example, if GaAs is deposited with epitaxy, Ga and As atoms are directed to a growth surface under ultra-high vacuum conditions. For growing III-V semiconductors,

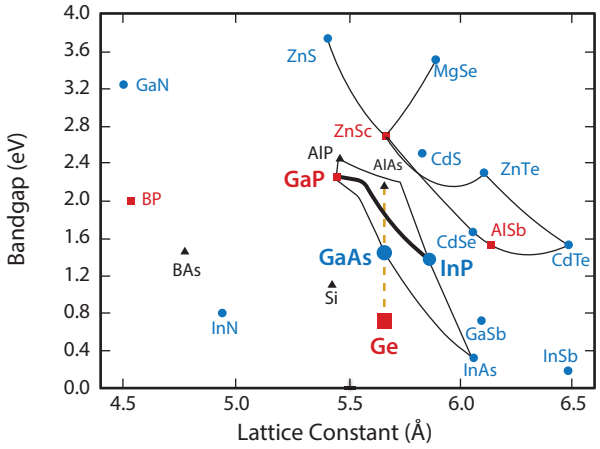

Figure 13.10: The bandgap and lattice constant of various III-V semiconductor materials.

germanium substrates usually are used. On this substrate the GaAs crystalline lattice is grown layer-by-layer and adopts the structure of the crystalline substrate.

As the layer-by-layer growth process is very slow, it allows the deposition of compact materials without any vacancy defects. Furthermore, processing at high vacuum conditions prevents the incorporations of impurities. Hence, III-V semiconductors can be deposited up to a very high degree of purity. Dopants can be added to make it *n*- or *p*-type.

Typically, III-V semiconductor layers are deposited by using *metal-organic chemical vapour deposition* (MOCVD). Typical precursor gasses are trimethylgallium [$Ga(CH_3)_3$], trimethylindium [$In(CH_3)_3$], trimehtylaluminium [$Al_2(CH_3)_6$] , arsine gas (AsH_3) and phosphine gas (PH_3). Surface reactions of the metal-organic compounds and hydrides, which contain the required metallic chemical elements, create the right conditions for the epitaxial crystalline growth. Epitaxial growth is a very expensive process; similar techniques are also used in the microchip production process.

A big challenge of depositing III-V semiconductor materials is that the lattice constants of the various materials are different, as seen in Fig. 13.10. We see that every III-V semiconductor has a unique bandgap-lattice constant combination. Hence, interfaces between different III-V materials show a lattice mismatch, as illustrated in Fig. 13.11. Because of this mismatch, not every valence electron is able to make a bond with a neighbour. This problem can be solved by *lattice matching*, as this also is done in the triple junction cell discussed in Section 13.2.1. For understanding what this means, we take another look at the phase diagram shown in Fig. 13.11. The triple junction is processed on a *p*-type germanium substrate, the bottom cell is a Ge cell. One top it is best to place a junction that has a higher bandgap but the same lattice constant. As we can see in the plot, GaAs has exactly the same lattice constant as Germanium. Therefore, between GaAs and Germanium interfaces can be made without any coordination defects related to mismatched lattices. For reasonable current density matching the desired bandgap of the top cell should be around 1.8 eV. However, we see that no alloys, based on solely two elements, exist. But if we take a mixture of gallium, indium and phosphorus, we can make a III-V alloys with a bandgap

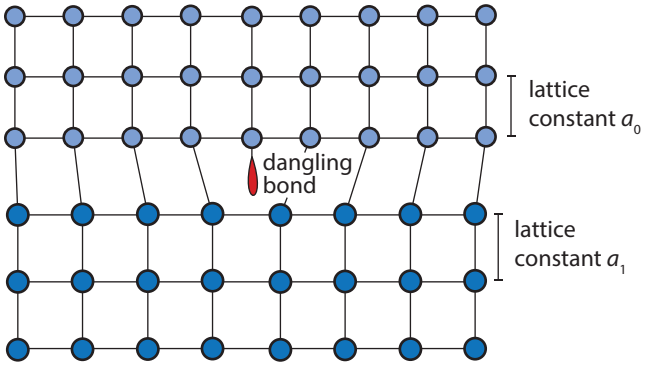

Figure 13.11: Illustrating the lattice mismatch at an interface between two different III-V materials.

of 1.8 eV material and with matching lattice constant. Consequently, triple junction cells based on GaInP, GaAs and Germanium can be fully lattice matched.

13.3 Thin-film silicon technology

In this section we will discuss thin-film silicon solar cells, which can be deposited on glass substrates and even on flexible substrates.

13.3.1 Thin-film silicon alloys

Thin-film silicon materials usually are deposited with *chemical vapour deposition* (CVD) processes that we will discuss in more detail in Section 13.3.3. In chemical vapour deposition different *precursor gasses* are brought into the reaction chamber. Due to chemical reactions, layer is formed on the substrate. Depending on the used precursors and other deposition parameters such as the gas flow rate, pressure, and temperature, various different alloys with different electrical and optical parameters can be deposited. We will discuss the most important alloys in the following paragraphs.

We start with two alloys consisting of silicon and hydrogen: *hydrogenated amorphous silicon* (a-Si:H) and *hydrogenated nanocrystalline silicon* (nc-Si:H), which is also known as microcrystalline silicon. The term *hydrogenated* indicates that some of the valence electrons in the silicon lattice are *passivated* by hydrogen, which is indicated by the ':H' in the abbreviation. The typical atomic hydrogen content of these alloys is from 5% up to about 15%. The hydrogen passivates most defects in the material, resulting in a defect density around 10^{16} cm^{-3} [66], which is suitable for PV applications. Often, the term 'hydrogenated' is left out for simplicity. Pure amorphous silicon (a-Si) would have an extremely high defect density ($> 10^{19}$ cm^{-3}) [67], which would result in fast recombination of photo-excited excess carriers. Similarly, we can make alloys from *germanium* and hydrogen: *hydrogenated amorphous germanium* (a-Ge:H) and *hydrogenated nanocrystalline germanium* (nc-Ge:H).